A computationally efficient method for determining the aerodynamic performance of kites for wind energy applications

Gaunaa, Mac; Paralta Carqueija, Pedro Filipe; Réthoré, Pierre-Elouan Mikael; Sørensen, Niels N.

Published in:
Proceedings

Publication date:
2011

Document Version
Publisher's PDF, also known as Version of record

A computationally efficient method for determining the aerodynamic performance of kites for wind energy applications

Mac Gaunaa, Pedro Filipe Paralta Carqueija, Pierre-Elouan Réthoré and Niels N. Sørensen
Wind Energy Department, Risø National Laboratory, DTU, DK-4000 Roskilde, Denmark
macg@risoe.dtu.dk

Abstract

A new computationally efficient method for determination of the aerodynamic performance of kites is proposed in this paper. The model is based on an iterative coupling between a Vortex Element Method (VLM) and 2D sectional airfoil coefficients to introduce the effect of airfoil thickness and effects of viscosity while retaining the strength of the VLM to model physically correct the effect of low aspect ratio and highly non-planar configurations. The performance of the new method will be assessed by comparison with simulation results from the state of the art incompressible Reynolds Averaged Navier-Stokes (RANS) solver EllipSys3D on a simplified kite-like geometry designed from lifting line theory.

1 Introduction

Several ideas of using kites as possible power sources emerged around the 70s and gradually along the years, but only until recently the research was intensified in this topic. Projects like the MS Beluga Skysails [1], where a container cargo ship sailed the Baltic Sea with the help of a secondary propulsion system consisting of a 160 m2 kite harvesting the energy in the wind and reducing, therefore, the fuel consumption; or stationary systems for electricity generation, such as the one presented originally by Loyd [2]. As an alternative to conventional wind turbines, the use of kites for harvesting power from the wind is a topic for several research groups [3–7]. With a kite it is possible to increase the line traction force by at least an order of magnitude compared to the steady case by making the kite perform crosswind motion. One way to harvest the energy in the wind using a kite is to generate electricity by letting a looping kite unroll a line from a drum connected to a generator. At the end of the production stroke, the kite is wound back to its initial position in a low traction force mode, from where the cycle can be repeated. The kite power generation technology is still in its infancy, and many open questions exist. Presently, it is not possible to give a realistic determination of either the power production or economic potential of such a system because there are too many unanswered questions on how to implement the basic ideas in real life. Critical key issues that have been spurred interest in academia include control [3, 5, 7–9], wind resources at high altitude [10], critical parameters for the mechanical energy output available [2, 4, 6, 11]. One of the areas where work is needed to get closer to be able to assess the potential of a kite power system is on the specific aerodynamic behavior/efficiency of the kites, including the effect of different key design features of the kite. Due to the relatively large number of inflow conditions (angle of attack and sideslip) and kite deformations (control actions and elastic deformations) that have to be considered in such an investigation, standard Computational Fluid Dynamics (CFD) methods such as Reynolds Averaged Navier-Stokes (RANS) modeling is too computationally costly. Therefore, the present work describe a new aerodynamic model based on a coupling between a Vortex Element Method (VLM) and 2D sectional airfoil coefficients to introduce the effect of airfoil thickness and effects of viscosity while retaining the strength of the VLM to model physically correct the effect of low aspect ratio and highly non-planar configurations. The performance of the new method will be assessed by comparison with simulation results from the state of the art incompressible RANS solver EllipSys3D [12–15] on a reference kite-like geometry designed using key results from classic lifting line theory [16]. Note that a big part of the present work was developed in connection with with the master thesis project by Carqueija [17], in which many of the present results can also be found.

2 Computational models

In this section, the computational models employed in this work are described.

2.1 New coupled prediction tool using geometry and 2D airfoil coefficients

The new model described in this work was inspired by the work of Horsten and Veldhuis [18], where...

Since one of the key elements in the model is a Vortex Lattice Method (VLM), this method is first described briefly.

2.1.1 Vortex Lattice Method

A few elements of the present method are worth mentioning but, for a full description of the method refer to e.g. [19].

The choice of using a VLM is due to its flexibility in incorporating changes of chord and twist distribution, and also because the VLM methods perform well at low aspect ratios. It consists of a distribution of vortex singularities over the discretized mean surface of the body (solutions of Laplace's equation, as mentioned previously) which allow the calculation of lift and induced drag. Thickness is neglected in this method which, however, incorporate the camber of the airfoil at each section. The condition of flow tangency to the mean surface determines the strengths of the vortex singularities.

The vortex singularities which, in the code used, consist of vortex rings, are placed at the quarter chord line of each panel. The advantage of such element is on the simple programming effort that it requires and on the fact that the boundary conditions can be exactly specified on the actual surface, which can take more complex shapes (ideal for kite investigations) [19]. The forces are calculated on each line element separately by applying the Kutta-Joukowsky theorem and then weighted to each of the collocation points. The calculation of the force is preceded by finding (i) the influence coefficients for each line element and (ii) the circulation, after solving the linear set of equations specifying the zero normal flow boundary condition.

In order to reduce the computational effort required to calculate the influence coefficients each time the inflow angle changes, the code incorporates an algorithm where only the coefficients related to the wake are updated, keeping constant the ones related to the geometry of the body. The change of inflow angle is incorporated in the right-hand side matrix (RHS), which includes the normal velocity components. For fine discretizations, this approach becomes extremely valuable as the calculation of influence matrices is a time consuming process.

As it will be presented, the algorithm is based on local geometric changes to account for viscosity. The problem rises due to the fact that, if geometry is changed, new influence matrices have to be computed each time the algorithm is run. The implementation in the present work encircles the problem by artificially changing the geometry of the body for each iteration of the algorithm. This is done by keeping the original geometry constant and applying the correspondent geometric change at each section by modifying the inflow angle at the section, changing the RHS vector. Figure 1 show that as the aspect ratio of an elliptic wing is increased, the results from the VLM method tends to the results of Prandtl's lifting line, which should be applicable for large aspect ratios.

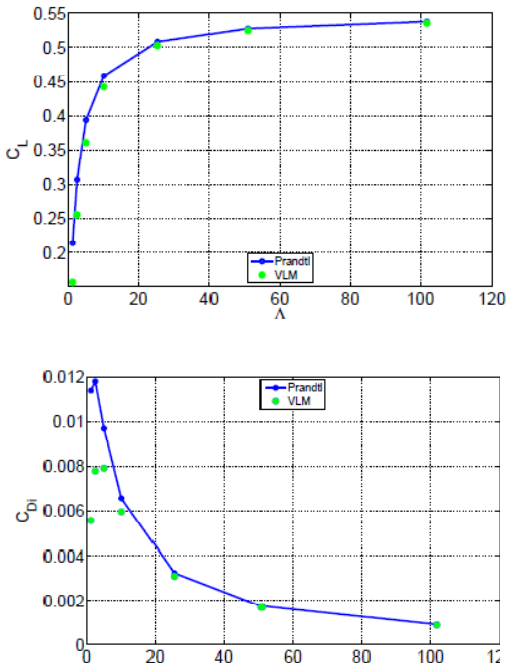

Figure 1: *VLM method validation against Prandtl's classical lifting line results for elliptically loaded wings. Upper: lift coefficient versus aspect ratio. Lower: induced drag coefficient versus aspect ratio.*

2.1.2 New coupling algorithm

Several approaches using two-dimensional data to account for viscous effects can be found in literature. The inspiration to the present algorithm is Horsten and Veldhuis' [18] formulation for wind tunnel interference correction, which uses the concept of 'morphed' wings to simulate viscosity along the lifting surface.

Figure 2 is needed to explain the present algorithm

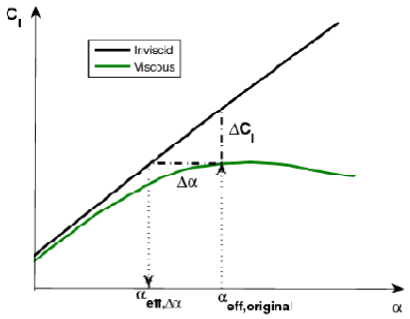

Figure 2: *Explanation of the coupling algorithm's baseline concept. The C_l is plotted versus α.*

The illustration shows the two-dimensional lift and drag coefficient curves for an assumed airfoil. For the effective angle of attack seen by a section - which is dependent of the downwash created by the trailing wake - the inviscid and viscous lift coefficients can be determined. To account for viscosity, a shift on the initial effective angle is performed so that, now, the airfoil works at an angle which has the same lift coefficient as the viscous lift coefficient before the angle shift.

$$C_{l_i}(\alpha_{eff_{\Delta\alpha}}) = C_{l_v}(\alpha_{eff_{original}}) \tag{1}$$

This angle shift is applied directly on the initial geometry of the lifting surface for the corresponding section. Now, changing the geometry, gives origin to a different loading on the body so there will be a new downwash value and, consequently, a new effective angle. An iteration procedure is required until the convergence of the angle shift value. This angle shift will, then, allow to calculate the viscous lift coefficient distribution along the body and, by integration, the total viscous lift coefficient. The total drag coefficient, on the other hand, is found by summing the induced drag coefficient for the updated geometry and the two-dimensional drag coefficient taken for the effective angle seen by each of the original sections (without the angle shift).

The VLM code incorporates two-dimensional viscous considerations on the solution, after external input of the spanwise drag coefficient vector, C_d. In other words, the code integrates along the span the two-dimensional C_d vector found with the coupling algorithm and adds the result to the total induced drag.

From thin airfoil theory we have

$$C^s_{l_i} = C_{l_\alpha} \cdot (\alpha^s_{eff}) \tag{2}$$

with,

$$\alpha^s_{eff} = \alpha_\infty + \alpha^s_{twist} - \alpha^s_0 - \alpha^s_i \tag{3}$$

$$C_{l_\alpha} = \frac{\partial C_l}{\partial \alpha} = 2\pi \tag{4}$$

α^s_i introduced already due to three-dimensional effects. As soon as the mentioned angle shift start to be applied on the lifting surface's initial geometry, the section lift coefficient changes until it converges. This final value, referred here as $C^s_{l_{i,final}}$, is expressed by the following

$$C^s_{l_{i,final}} = C_{l_\alpha} \cdot \left(\alpha_\infty + \alpha^s_{twist} - \alpha^s_0 - \alpha^s_{i,final} - \frac{\Delta C^s_l\left(\alpha^s_{eff,final}\right)}{C_{l_\alpha}}\right) \tag{5}$$

In equation 5, $\alpha^s_{i,final}$ is the final induced angle, for the converged angle shift given by the last term of the equation. Subtracting equations 2 and 5 results in,

$$\begin{aligned} C^s_{l_{i,original}} - C^s_{l_{i,final}} &= \\ C_{l_\alpha} \cdot \left(\alpha^s_{i,final} \right. &- \left. \alpha^s_{i,original}\right) \\ +\Delta C^s_l(\alpha_\infty + \alpha^s_{twist} &- \alpha^s_0 - \alpha^s_{i,final}) \\ = C_{l_\alpha} \cdot \left(\alpha^s_{i,final} \right. &- \left. \alpha^s_{i,original}\right) \\ +\Delta C^s_l(\alpha_\infty + \alpha^s_{twist} &- \alpha^s_0 \\ -\alpha^s_{i,original} &- (\alpha^s_{i,final} - \alpha^s_{i,original})) \end{aligned} \tag{6, 7}$$

$C^s_{l_{i,original}}$ being the lift coefficient taken from the first calculation with no angle shift applied. Reorganizing yields,

$$\Delta\alpha^s_i = \alpha^s_{i,final} - \alpha^s_{i,original} = \frac{C^s_{l_{i,original}} - C^s_{l_{i,final}}}{2\pi} - \Delta\alpha^s \tag{8}$$

$$\Delta\alpha^s = \frac{\Delta C^s_l\left(\alpha_\infty + \alpha^s_{twist} - \alpha^s_{i,original} - \left(\alpha^s_{i,final} - \alpha^s_{i,original}\right)\right)}{C_{l_\alpha}} \tag{9}$$

The difference between induced angles, $\Delta\alpha_i^s$, in equation 8 can then be determined without computing the induced angles themselves.

As for the two-dimensional drag coefficients, the values are taken for

$$C_d^s = C_d\left(\alpha_{eff_{original}}\right) = C_d\left(\frac{C_{l_{i,original}}^s}{C_{l_\alpha}} + \alpha_0^s\right) \tag{10}$$

From the relations above, the algorithm can be structured as follows:

1. VLM is called and the $C_{l,i,original}^s$ for each section along the span is saved. This first value is considered as being the baseline, original value.
2. Initialize $\Delta\alpha_i^s$ as equal to zero
3. Find α_{eff}^s for each section, from:

$$\alpha_{eff}^s = \frac{C_{l_{i,original}}^s}{C_{l_\alpha}} + \alpha_0^s - \Delta\alpha_i^s \tag{11}$$

4. Calculate $\Delta C_l^s = \Delta C_l(\alpha_{eff}^s)$
5. Calculate $\Delta\alpha^s$, from:

$$\Delta\alpha^s = \frac{\Delta C_l^s}{C_{l_\alpha}} \tag{12}$$

6. Call VLM with the artificial angle correction, $\Delta\alpha^s$, and save for each section along the span the new lift coefficient, $C_{l,i,final}^s$
7. Calculate $\Delta\alpha_i^s$ using Equation 8
8. Return to step 3 until convergence

Convergence is controlled through the residual value between the $\Delta\alpha_i^s$'s of the two last iterations. The iteration process runs until the condition

$$\epsilon^s = max(\left|\Delta\alpha_{i,k}^s - \Delta\alpha_{i,k-1}^s\right|) \leq 10^{-3} \tag{13}$$

is satisfied, for iteration k.

For a certain predetermined number of iterations, if the results have not converged, a *Sucessive Over Relaxation method* is applied to fasten up convergence.

Several differences can be pointed between the approach in [18] and the present algorithm:

1. Iteration is introduced in the present algorithm to ensure that the induced drag is based on the correct loading.
2. The computation of the induced angles is avoided. As a note, it is known from theory that the wake should be force free. However, not computing it properly can lead to wrong calculations of the induced drag force on the body and, consequently, the induced angles [19]. The potential flow code used assumes a prescribed wake model and, therefore, it is better to not calculate induced angles.
3. The two-dimensional form drag coefficients are calculated for the initial effective angle corresponding to the original lift distribution, and not to the shifted effective angle, as in [18]. The reason is that the actual angle seen by the lifting surface is still the original effective angle, $C_{l,original}$, without any angle shifts. The shift in geometry serves only the purpose to match the viscous lift distribution to the inviscid one.

2.2 Computational Fluid Dynamics: EllipSys3D

2.2.1 Method

The in-house flow solver EllipSys3D [12–15] is used in all CFD computations presented in the following. The EllipSys3D code is a multiblock finite volume discretization of the incompressible Reynolds-averaged Navier-Stokes (RANS) equations in general curvilinear co-ordinates. The code uses a collocated variable arrangement, and Rhie/Chow interpolation [20] is used to avoid odd/even pressure decoupling. As the code solves the incompressible flow equations, no equation of state exists for the pressure, and the SIMPLE algorithm of Patankar and Spalding [21] is used to enforce the pressure/velocity coupling. The EllipSys3D code is parallelized with MPI for execution on distributed memory machines, using a non-overlapping domain decomposition technique. The solution is advanced in time using a second-order iterative time-stepping (or dual time-stepping) method. In each global time step the equations are solved in an iterative manner, using underrelaxation. First, the momentum equations are used as a predictor to advance the solution in time. At this point in the computation the flow field will not fulfil the continuity equation. The rewritten continuity equation (the so-called pressure correction equation) is used as a corrector to make the

predicted flow field satisfy the continuity constraint. This two-step procedure corresponds to a single subiteration, and the process is repeated until a convergent solution is obtained for the time step. When a convergent solution is obtained, the variables are updated and the computation continues with the next time step. For steady state computations the global time step is set to infinity and dual time stepping is not used. This corresponds to the use of local time stepping. To accelerate the overall algorithm, a three-level grid sequence is used in the steady state computations. The convective terms are discretized using a third-order upwind scheme, implemented using the deferred correction approach first suggested by Khosla and Rubin [22]. In each subiteration, only the normal terms are treated fully implicitly, while the terms from non-orthogonality and the variable viscosity terms are treated explicitly. Thus, when the subiteration process is finished, all terms are evaluated at the new time level. The three momentum equations are solved decoupled using a red/black Gauss-Seidel point solver. The solution of the Poisson system arising from the pressure correction equation is accelerated using a multigrid method. In the present work the turbulence in the boundary layer is modelled by the $k-\omega$ SST model of Menter [23]. The equations for the turbulence model are solved after the momentum and pressure correction equations in every subiteration/pseudo time step. In the present work, all computations are performed using a $\gamma - \widetilde{Re}_\theta$ Laminar-turbulent transition model [24].

2.2.2 Mesh

The central part of the blades have a spanwise discretization of the mesh points following a tangent hyperbolic distribution. The roots and the tips surfaces of each blades are meshed using the commercial software Pointwise to generate the surface fitted domains. The 3D mesh generation is done with a 3D version of hypgrid [25] an in-house hyperbolic mesh generation code. Some illustrations of the mesh generation on mesh are illustrated in Fig.3.

2.2.3 Boundary Conditions

A zero gradient is enforced normal to the outlet of the downstream end of the spherical domain

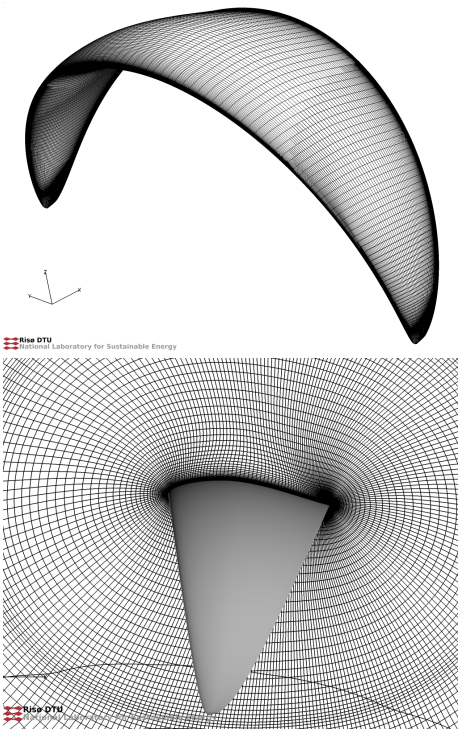

Figure 3: *Details of the computational mesh.*

where the flow leaves the domain. At the upstream part of the spherical domain the undisturbed wind speed is specified. The surface of the blades are set as wall (no-slip) boundary conditions.

3 Reference Kite Geometry

In order to develop a reference geometry with which to test the developed code, it was chosen to make a shape with the crossectional section consisting only of one single airfoil type. The sectional shape of this is the NACA 64-418 section [26]. In order to have a planform which performs well in at least one point, a design was based on the classical lifting line results of Munk [16]. Munk's analysis showed that the solution that leads to the system of trailed vorticity for which the induction in the direction perpendicular to the projection of the wing on the Trefftz plane is proportional to the cosine of the wing angle minimizes the induced drag.

Since the trailed vorticity is equal to the change in bound vorticity along the wing it is a straightforward task to determine the induced velocities in the direction perpendicular to the trailed vortex sheet at the Trefftz plane. Due to the linearity of the problem result in a linear

system which can be written as

$$\vec{\mathbf{A}}\vec{\Gamma}_b = \vec{V}_p \tag{14}$$

Here, the $\vec{\mathbf{A}}$ matrix will depend only on the geometry of the lifting line. $\vec{\Gamma}_b$ is a column vector holding the bound vorticity, and $\vec{V}_p$ is the induced velocities in the Trefftz-plane normal to the intersectional curve. Munks condition for minimum induced drag can be written

$$\vec{V}_p = \cos(\vec{\Theta})K \tag{15}$$

where $\vec{\Theta}$ is the vector with the inclination of the wing, and K is a constant. Upon combining Equations (14) and (15), we see that the bound vorticity of the case which minimizes induced drag for a given lift will be

$$\vec{\Gamma}_b = \vec{\mathbf{A}}^{-1}\cos(\vec{\Theta})K \tag{16}$$

Here we see that K is simply the scaling factor that determines the level of the bound circulation. We also see that the distribution shape of it is otherwise constant, given by the shape of the wing. When the definition of the 2D lift coefficient

$$C_l = \frac{l}{0.5\rho V_\infty^2 c} \tag{17}$$

is combined with the locally lifting part of the Joukowski equation

$$l = \rho V_\infty \Gamma_b \tag{18}$$

we get an expression for the chordlength on the wing as

$$c = \frac{2\Gamma_b}{V_\infty C_l} \tag{19}$$

Combining this local expression for the chordlength with the expression for the optimal bound circulation, Equation (16), we can therefore get the expression for the chordlengths for the whole wing as

$$\vec{c} = \frac{2\vec{\mathbf{A}}^{-1}\cos(\vec{\Theta})}{V_\infty C_l}K \tag{20}$$

Again, we see that if we choose a design lift coefficient, the constant K simply scales the chordlengths on the rotor. This way once the geometry of the line that defines the span in space is determined, we are now able to determine the distribution of chordlengths along that span using Equation (20). The constant K which corresponds to the desired mid chord length, or wing aspect ratio can then be picked.

Once K is chosen, the corresponding bound vorticity can be evaluated using Equation (16), and from this and the layout of the wing lifting line in space, the induced velocities from the trailed vortices at the location of the lifting line can be determined. This enables the determination of the direction of the chordlengths in space using the design angles of attack corresponding to the design lift coefficient and the airfoil section.

Using the wing layout procedure described above with the elliptic shape (half-ellipse of total with 1 and height 0.4) of the span in space depicted in Figure 4. The figure also show chord distribution (mid-chord length of 0.3) and local twist of the wing, which has the NACA 64-418 airfoil as crossection.

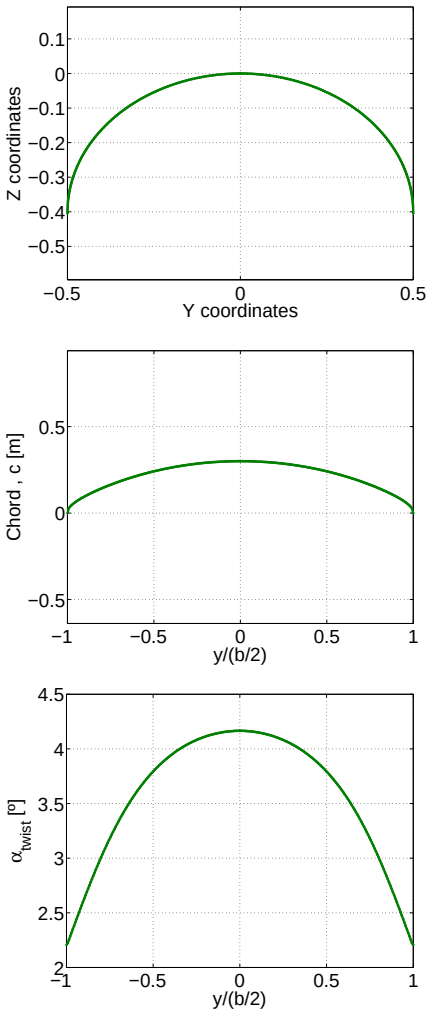

Figure 4: *Layout of the reference kite geometry. Upper: layout of the wing span in space (x-coordinate=default wind direction, is zero). Middle: Chordlength. Lower: Local twist of the wing.*

4 Results

CFD computations were carried out on the reference kite at a range of inflow conditions, both pitch angles and sideslip angles. Figure 5 show examples of the predicted flowfields, where the complex nature of the flow situations are visible.

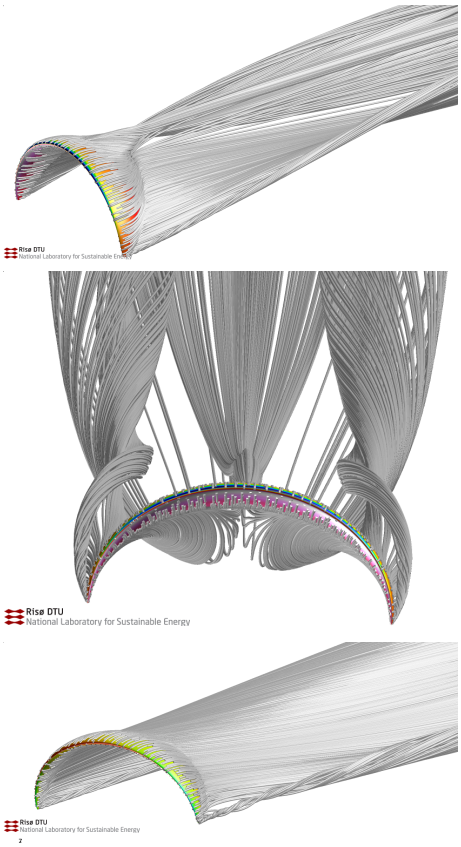

Figure 5: *Visualizations of the predicted flowfield around the kite using CFD. Upper and middle:* $\alpha_{pitch} = 12^0$, $\beta_{sideslip} = 0^0$. *Lower:* $\alpha_{pitch} = 0^0$, $\beta_{sideslip} = 8^0$

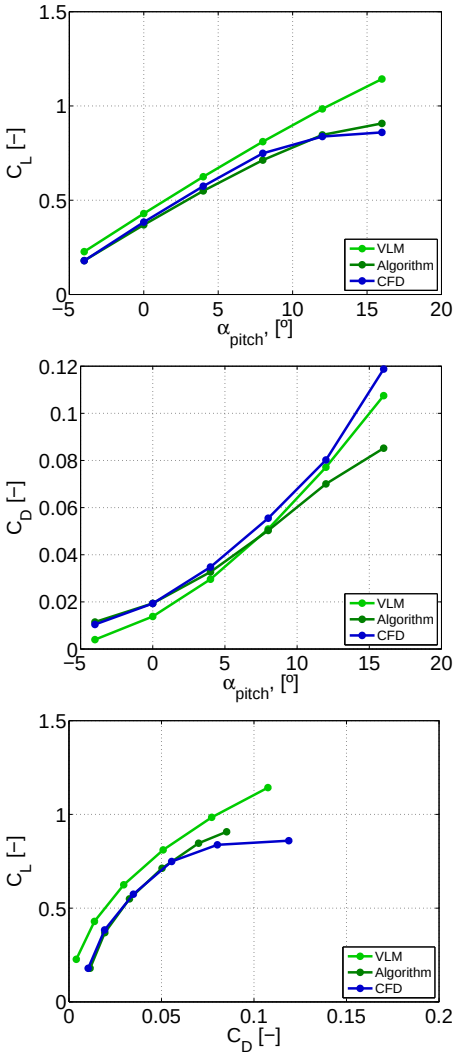

Figure 6: *Comparison of lift and drag coefficients simulated on the reference kite at zero sideslip angle. Upper:* C_L *versus pitch angle. Middle:* C_D *versus pitch angle. Lower:* C_L *versus* C_D.

4.1 Zero sideslip angle

Comparison of the integral computational results obtained with the raw VLM, the new coupled method and the CFD results for the reference kite at zero sideslip angle is shown in Figure 6.

It is seen that the performance of the new coupled model is very good. The model captures the beginning of stall well on lift, and the drag for which the flow is attached is predicted in very close agreement with the CFD results. The underprediction of the drag does not set in before $\alpha_{pitch} = 8^O$. Please bear in mind that this angle is the inclination of the onset flow relative to the design point of the reference kite, so the flow angle relative to the kite is more than zero when $\alpha_{pitch} = 0^0$. Overall the performance of the model is found to be very good for these cases.

It should be noted that until a time stepping simulation of a kite system, using for instance tabulated data from the present model, has been performed, it is not clear what the typical operational conditions is for a kite. It is very likely, however, that situations with stall will be avoided, because the lowered lift to drag values in this case results in much lower kite velocities, which again results in lower than optimal kite traction forces.

4.2 Sideslip angle

Figure 7 show the performance of the models for cases with sideslip angles different from zero.

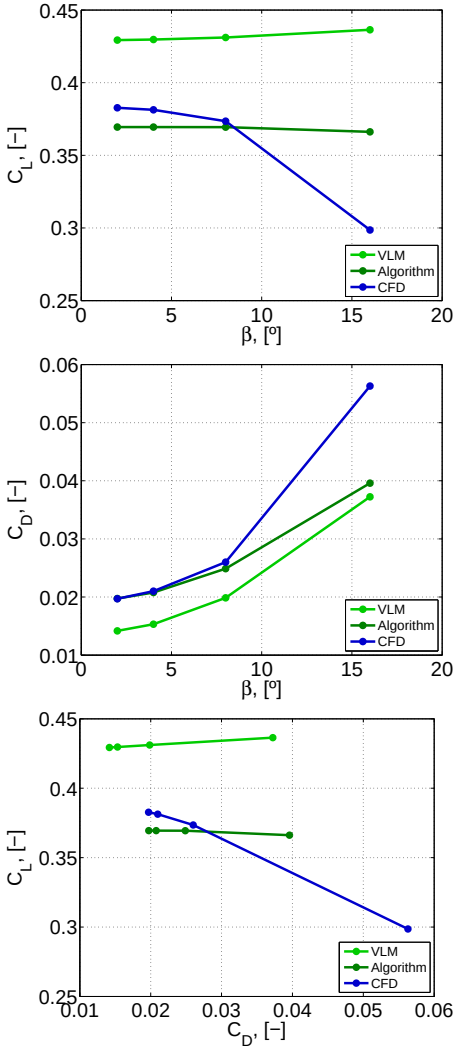

Figure 7: *Comparison of lift and drag coefficients simulated on the reference kite for sideslip angles. Upper:* C_L *versus angle of attack. Middle:* C_D *versus angle of attack. Lower:* C_L *versus* C_D*.*

As in the previous case, the agreement between CFD and the new algorithm in the region where the flow is not stalling is excellent. As the sideslip angle is increased the agreement deteriorates somewhat. As was mentioned previously, the typical operational conditions is for a kite are unknown, but likely to remail attached for the majority of the time. Therefore it is likely that the present model could provide aerodynamic data useful for detailed analysis of kite energy systems.

4.3 Computational time

The ratio between computational times used for the same number of cases for the new algorithm and the CFD method is approximately $1/400$.

5 Conclusions and further work

The present report contains description of a new, computationally light, algorithm, which can determine the aerodynamic loading on a kite for wind energy applications. The model couples a Vortex Lattice Method with 2D airfoil data iteratively to take into account effects of airfoil thickness and effects of viscosity.

The computational time of the new coupled algorithm is approximately $1/400$ of the time of the state of the art CFD prediction tool EllipSys3D.

The agreement between the present model and the CFD results is excellent for cases where the flow remains attached over the kite. The agreement deteriorates as the flow enters the stalled state.

As the typical operational conditions is for a kite in a kite power system are unknown, but likely to remain attached for the majority of the time, it is likely that the present model can provide aerodynamic data useful for detailed analysis of kite energy systems.

Further work Further work include

- Further validation of the new model with crossection shapes closer to what is found on real kites.
- Development of a time stepping tool which builds on a database of results produced with the present method.
- Investigation of the effect of line drag, control strategies, etc. using a database with aerodynamic results from the present method
- Investigations of what a 'good' kite design is (effect of design choices of the kite layout)
- More realistic determination of the power production capabilities of a kite power system using performance characteristics for a realistic kite simulated using the present coupled method

- Investigation of the effect of extreme events (shear, gusts).
- Fatigue analysis of specific key elements in a kite power system.

Based on the results presented in the paper, the envisaged further work is therefore a detailed investigation of design choices of the kite, control system design (sensor, actuator, control algorithms for both generator and flight path), line specifications, effect of extreme events (shear, gusts) and fatigue analysis of specific key parts of the kite energy system.

Acknowledgements

It is gratefully acknowledged that the work in this paper was heavily helped by all the inspirational discussions we had with the Kitemill guys: Olav Aleksander Bu, Thomas Hårklau, Eric Beaudonnat and Bruno Legaignoux.

References

[1] SkySails. *http://www.skysails.info/*

[2] M.L. Loyd. *Crosswind Kite Power.* Energy, Vol 4, 3, p. 106-111. 1980.

[3] P. Williams and B. Lansdorp and W. Ockels *Optimal Crosswind Towing and Power Generation with Tethered Kites.* Journal of Guidance, Control and Dynamics, Vol 31, 1. 2008.

[4] G.M. Dadd and D.A. Hudson and R.A. Shenoi. *Comparison of Two Kite Force Models with Experiment.* Journal of Aircraft. Vol 47, 1. 2010.

[5] M. Canale and L. Fagiano and M. Milanese. *Power Kites for Wind Energy Generation: Fast Predictive Control of Tethered Airfoils.* IEEE Control Systems Magazine. 2007

[6] I. Argatov and P. Rautakorpi and R. Silvennoinen. *Estimation of the mechanical energy output of the kite wind generator.* Renewable Energy. Vol 34, p 1525-1532. 2009.

[7] B. Houska and M. Diehl. *Optimal Control for Power Generating Kites.* Proceedings of the 45th IEEE Conference on Decision and Control. p. 2693-2697. 2006.

[8] P. Williams and D. Sgarioto and P.M. Trivailo *Constrained Path-planning for an Aerial-Towed Cable System.* European Conference for Aerospace Sciences (EUCASS). 2006

[9] A.R. Podgaets and W.J. Ockels. *Three-dimensional simulation of a Laddermill.* Proceedings of the 3. Asian Wind Power Conference. 2006.

[10] C.L. Archer and K. Caldeira *Global Assessment of High-Altitude Wind Power.* Energies. Vol 2, p. 307-319. 2009.

[11] I. Argatov and R. Silvennoinen. *Energy conversion efficiency of the pumping kite wind generator.* Renewable Energy. Vol. 35. p 1052-1060. 2009.

[12] Michelsen J.A. *Basis3D - a Platform for Development of Multiblock PDE Solvers.* Technical Report AFM 92-05, Technical University of Denmark, 1992

[13] Michelsen J.A. *Block structured Multigrid solution of 2D and 3D elliptic PDE's.* Technical Report AFM 94-06, Technical University of Denmark, 1994

[14] Sørensen N.N. *General Purpose Flow Solver Applied to Flow over Hills.* Risø-R-827-(EN), Risø National Laboratory, Roskilde, Denmark, June 1995

[15] Sørensen N.N., Michelsen J.A., Schreck, S. *Navier-Stokes predictions of the NREL phase VI rotor in the NASA Ames 80 ft X 120 ft wind tunnel.* Wind Energy. 2002;5(2-3):151-169.

[16] M.M. Munk. *The Minimum Induced Drag of Aerofoils.* NACA Technical Report R-121. 1923.

[17] P.F.P. Carqueija. *Aerodynamic Investigations of a High-altitude Wind Energy Extraction System.* MSc Thesis. Instituto Superior Tecnico, Universidade Tecnica de Lisboa. October 2010.

[18] B.J.C. Horsten and L.L.M. Veldhuis *A New Hybrid Method to Correct for Wind Tunnel Wall and Support Interference On-line.* World Academy of Science, Engineering and Technology, Vol 58. 2009.

[19] J. Katz and A. Plotkin *Low-Speed Aerodynamics - From Wing Theory to Panel Methods.* Second Edition. Cambridge University Press. 2001.

[20] Rhie, C.M. *A numerical study of the flow past an isolated airfoil with separation*. PhD thesis, Univ. of Illinois, Urbana-Champaign, 1981.

[21] Patankar, S.V. and Spalding, D.B., *A Calculation Prodedure for Heat, Mass and Momentum Transfer in Three-Dimensional Parabolic Flows.* Int. J. Heat Mass Transfer, 15:1787, 1972.

[22] Khosla, P.K. & Rubin, S.G. *A diagonally dominant second-order accurate implicit scheme.* Computers Fluids, 2:207–209, 1974.

[23] Menter, F.R. *Zonal Two Equation k-ω Turbulence Models for Aerodynamic Flows*. AIAA Paper 93-2906, 1993

[24] Sørensen, N.N. *Cfd modelling of laminar-turbulent transition for airfoils and rotors using the gamma-(re)over-tilde (theta) model.* Wind Energy, 12(8):715–733, 2009.

[25] Sørensen, N.N., *HypGrid2D, a 2-D mesh generator.* Technical report, Risø-R-1035(EN), Risoe National Laboratory, 1998.

[26] Abbott, I.H. & von Doenhoff, A.E. *Theory of Wing Sections, including a summary of airfoil data* Dover, 1949.